Composites Science and Technology 149 (2017) 149–158

Contents lists available at ScienceDirect

Composites Science and Technology

journal homepage: http://www.elsevier.com/locate/compscitech

Subtle features of delamination in cross-ply laminates due to low speed impact

Elena Sitnikova [a, *], Shuguang Li [a], Dafei Li [a], Xiaosu Yi [b]

[a] Faculty of Engineering, The University of Nottingham, University Park, Nottingham, NG7 2RD, UK
[b] Beijing Institute of Aeronautical Materials, Wenquan, Haidian District, Beijing, 100095, China

ARTICLE INFO

Article history:
Received 8 March 2017
Received in revised form
14 June 2017
Accepted 20 June 2017
Available online 21 June 2017

Keywords:
Laminate
Delamination
Matrix cracking
Damage mechanics
Friction

ABSTRACT

In cross-ply laminates, the shape of delamination areas, which form due to low velocity impact, have two subtle features, which have been observed consistently in numerous experiments. Those are the pointed delamination tips and the intact zone between the lobes of delamination. However, there have not been any account available in the literature how they can be consistently captured through numerical modelling, and hence these features in published modelling results were often absent. It is the objective of this paper to identify the underlying modelling considerations so that these features can be captured with confidence. A key and unique reason has been identified in each case. Namely, inclusion of intra-laminar damage allows to reproduce the pointed delamination tips, while the gap between the lobes of delamination can be captured by models with sufficiently refined mesh, where friction between the laminas is taken into account. The capability of capturing these subtle features helps to raise the level of fidelity on the simulation of delamination due to impact.

1. Introduction

Delamination in laminated composites caused by low speed lateral impact has been subjected to countless investigations from various perspectives [1], to such an extent that standards [2] have been drawn, as the problem has been considered as one of the key aspects in material selection, in particular, for aerospace applications.

Cross-ply laminates are one of the simplest types of laminates, which is not of much practical significances in terms of their engineering applications. However, their simplicity makes them an ideal case of verifications and validations of theoretical models. They have indeed been employed frequently as one of the benchmarking cases [3]. Experimental results based on different materials are found highly reproducible and consistent [4–6]. Most of the prominent features of delamination are captured well through carefully conducted numerical simulations. Reasonable agreement between the experimentally observed and numerically predicted delamination, both qualitative and quantitative, has been reported by many [5,7–10]. More research outcomes are still being reported [11–16], which suggests the need of better understanding before composites can be applied with higher level of fidelity, the lack of which in relation to the extensive use of composites in Boeing 787 was clearly identified in the report from a US government public enquiry [17].

In order to improve modelling of the delamination predictions under low velocity impact, different considerations are taken into account. Some researchers seek to improve the formulation of the constitutive behaviour of the cohesive layers, proposing modifications to the existing models [18] or devising models of their own [15]. Specifically, in their recent review, Abrate et al. [19] surveyed a great variety of cohesive zone models available to-date.

Accounting for the intra-laminar damage is yet another aspect which is commonly included into the formulations of the models. Again, both the material models available in commercial finite element codes [11,13] and the user-defined models [5,16] have been used for the purpose.

Another consideration, which is sometimes included in the formulation of the models, is the effect of friction on contact surfaces between the adjacent delaminated laminae following the failure of the interface [4,5,13–16].

Though a reasonable agreement between the experiment and modelling is usually reported, there is still lack of understanding as to what effect the various factors included in modelling have on

* Corresponding author.
E-mail address: elena.sitnikova@nottingham.ac.uk (E. Sitnikova).

http://dx.doi.org/10.1016/j.compscitech.2017.06.021
0266-3538/

delamination predictions. Another closely associated and even more important issue is the inability to comprehensively explain two subtle features of delamination as will be defined below, which are observed consistently in impact tests of cross ply laminates, but are not captured in many accounts exploring the subject.

Consider the relatively best known case of cross-ply laminates of a layup $[0^\circ_m/90^\circ_n/0^\circ_m]$ subjected to impact, as defined by ASTM standard [2]. It can be easily predicted, as well as experimentally observed, that little delamination occurs on the $0^\circ/90^\circ$ interface closer to the impactor, and the observed delamination is dominated by the one on the $90^\circ/0^\circ$ interface farther from the impactor. The delamination area and dimensions are always measured from the dominant delamination. Schematic drawing of the delamination outline as typically observed experimentally is shown in Fig. 1. The following two subtle features as marked have never been understood appropriately and captured consistently through modelling.

(1) The tips of delamination at both ends tend to be pointed;
(2) The intact zone between the two lobes of the delamination. The so-called intact zone is usually not entirely damage free. In fact, complicated damage patterns can usually be observed there as a result of localised indentation due to the impact. However, as far as the interface under consideration is concerned, the delamination does not propagate into this zone.

Researchers tend to turn a blind eye to them when producing their theoretical predictions, hence even when captured in some way [15,16,20], the comprehensive explanation of the definitive factors in the modelling responsible for those subtle features has never been given. There is no lack of interest in capturing these features as they are so characteristic and experimentally reproducible, but the fact is that there has been not yet a conclusive statement about their being and the reason behind such distinctive features of delamination. Although such subtle features are not as significant as the delamination area and dimensions in representing the effects of the delamination, the inability to capture them does cast doubts on the fidelity of predictions, even if one has managed to estimate the area and the dimensions reasonably accurately. Without capturing such consistently observable features, the authors would find it hard to be content with the existing simulation capability.

The objective of this paper is to address these subtleties. The discussion is restricted to $[0_3/90_3]_s$ layup, in which the two subtle features as discussed are always present, as confirmed by numerous experimental studies. It has been revealed that they result from definitive reasons and, once these reasons have been taken into account properly, these subtle features can be captured consistently in numerical simulations. The authors have been inspired by available results and considerations in the literature, such as generic mesh sensitivity of the problem and contributions from the effects of transverse matric cracking and the delaminated interfacial friction. However, there has been no account available in the literature, to the best of the authors' knowledge, where such considerations have been associated specifically with the features under investigation in this paper. Through the specific considerations introduced to the model as presented in this paper, these subtle features will be reproduced vividly and reasons responsible for these features will be identified.

2. Modelling cross-ply laminates subjected to impact

In the present investigation, delamination due to low velocity impact on cross-ply laminate of $[0_3/90_3]_s$ lay-up is studied via finite element modelling conducted with Abaqus/Explicit [21]. The finite element model was generated in order to compare directly with the laminated panel impact experiments [6,10]. The model takes into account effects of both the intra-laminar cracking, through a user-defined material subroutine for the composite laminas, and the delamination at the interfaces, which is modelled using conventional cohesive elements as available in Abaqus.

2.1. Finite element model

In the experiments [6], the $[0_3/90_3]_s$ laminate was 2 mm thick, with 65 mm $\times$ 87.5 mm in-plane dimensions. The laminate panel was simply supported. The simple support conditions in the experiments were obtained by resting the specimen on a rigid steel frame with a rectangular opening of dimensions 45 mm $\times$ 67.5 mm with all four corners of the specimen clamped to the frame. The clamps were to ensure zero deflection at the corners. The specimen was impacted at the centre by a hemispherical impactor 12.5 mm in diameter, which was considered as a rigid body. Impacts of different energies were simulated by assigning appropriate velocity values to the impactor at the instant of contact. The mass of the impactor in the tests was 2.3 kg.

To reduce the computational costs, only a quarter of the specimen was modelled, with appropriate symmetry conditions being imposed, as specified in Fig. 2(a). The composite laminate was idealised into a layup of three laminae, each consisting of plies having a common orientation as shown in Fig. 2(b). The interfaces between the composite layers were modelled using cohesive elements COH3D8. The unidirectional composite layers were meshed with continuum shell elements, SC8R. The surface-to-surface contact interactions were defined between the plate and the indenter. The same were also pre-planted on the faces of neighbouring laminae, which would be activated upon the deletion of the cohesive elements following interface failure to prevent the interpenetration between the neighbouring laminae. Since the analysis was conducted with a quarter of the panel, the mass of the impactor was also reduced to a quarter in the model.

Given the mesh sensitivity of delamination problems in general, a study has been conducted to determine the mesh convergence, which was reached when both the composite and the cohesive layers were meshed with elements of 0.25 mm $\times$ 0.25 mm in-plane

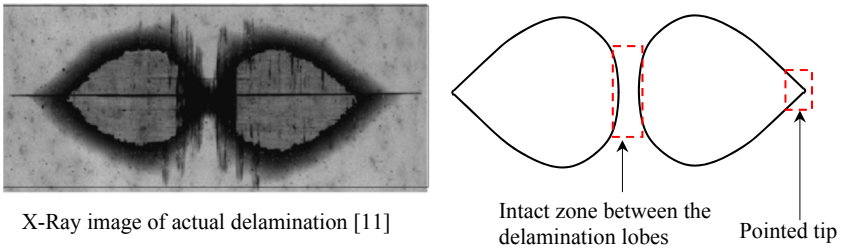

Fig. 1. X-Ray image of actual delamination and a schematic drawing of the delamination pattern typically observed experimentally.

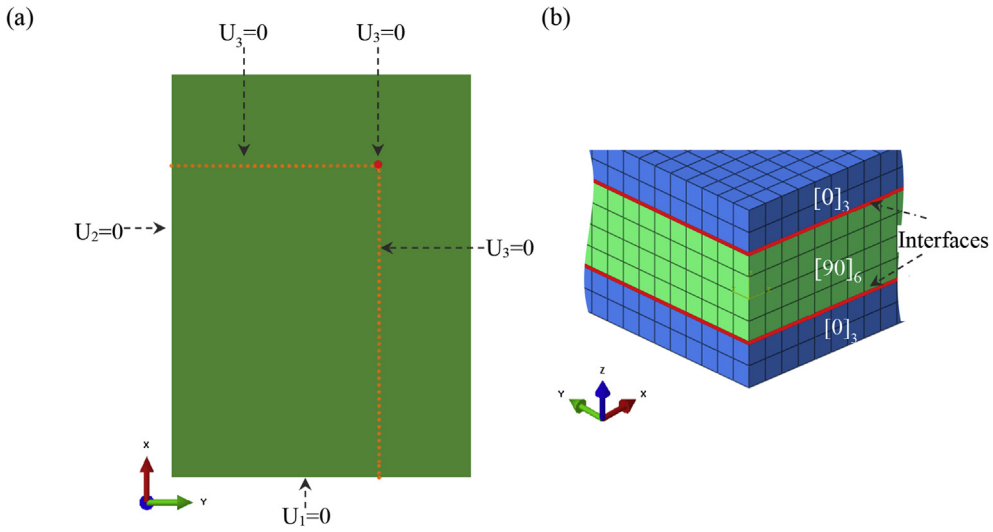

Fig. 2. Finite element model of the laminate: (a) bottom view of the quarter panel with the boundary conditions indicated (b) close-up view of the mesh around the centre of the panel.

dimensions and the through-the-thickness arrangement as shown in Fig. 2(b). This mesh was applied in most cases presented, except for a specific consideration as will be elaborated later in this paper.

2.2. Constitutive model for the composite lamina taking account of intra-laminar damage

Cracking in unidirectional composites (UD) was apparent in the experiments [6], where damage occurred in form of cracks in both the 90° lamina and the 0° lamina on the distal side of the impactor. In particular, a discrete transverse matrix crack has been observed in that 0° lamina, running through the centre of the lamina. In addition to that, numerous dispersed micro-cracks can also be easily seen in X-ray images of tested laminates. The effects of dispersed damage results in stiffness reduction, which can be described reasonably reliably using a continuum damage mechanics (CDM) model. In the present work, damage model developed by the second author and his co-workers, and validated extensively [22,23] previously, has been adopted for this purpose.

The constitutive relationship for the laminae is given as follows.

$$\{\sigma\} = [Q]\{\varepsilon\}, \tag{1}$$

where Q is the laminar stiffness matrix which is in general a function of damage variable, ω.

An incremental form of Eq. (1) is obtained as

$$\{d\sigma\} = [Q^t]\{d\varepsilon\}, \tag{2}$$

where

$$\begin{aligned} [Q^t] &= [Q^\omega] + \frac{[Q^\omega]\{\varepsilon\}\dfrac{\partial F}{\partial\{\sigma\}}[Q^\varepsilon]}{h\eta\omega^{\eta-1} - \dfrac{\partial F}{\partial\{\sigma\}}[Q^\omega]\{\varepsilon\}}, \\ Q^\varepsilon_{ij} &= Q_{ij} + Q'_{ij}\omega, \\ Q^\omega_{ij} &= Q'_{ij} \quad (i,j = 1,2), \\ Q^\varepsilon_{66} &= (1 - k\omega)G \text{ and } Q^\omega_{66} = -kG. \end{aligned} \tag{3}$$

In Eq. (3), G is the elastic in-plane shear modulus of virgin material and k is a damage-related laminate constant [22]. The expressions for Q_{ij} and Q'_{ij} in terms of conventional elastic constants can be found in Ref. [23] as a simplified version of continuum damage representation proposed by Talreja [24].

For simplicity, the damage initiation was defined via the maximum stress failure criterion, which is written as follows.

$$F(\sigma) = \frac{\sigma_2}{\sigma_{2c}} \tag{4}$$

where σ_{2c} is the transverse strength within the lamina.

The evolution of damage is given in an incremental form as [23].

$$d\omega = \left(h\eta\omega^{\eta-1} - \frac{\partial F}{\partial\{\sigma\}}[Q^\omega]\{\varepsilon\}\right)^{-1}\frac{\partial F}{\partial\{\sigma\}}[Q^\varepsilon]\{d\varepsilon\}. \tag{5}$$

It was derived based on the concept of the damage surface, which was defined in the following form [23].

$$f(\sigma,\omega) = (1 + h\omega^\eta)^{-1}F(\sigma) = 1, \tag{6}$$

where h and η are properties of the material of lamina associated with the size effects of the material. Unloading is characterised by $d\omega$ becoming negative, in which case Eqs. (3) and (5) are replaced by

$$[Q^t] = [Q^\varepsilon] \text{ and } d\omega = 0. \tag{7}$$

The elastic constants and other relevant material properties of the composite are listed in Table 1. To define the response of the material with the damage, two additional quantities, h and η, need to be specified.

The damage model was implemented as a user-defined VUMAT subroutine. To verify the damage model implementation, typical material responses under transverse loading were calculated based on a single element model. In Fig. 3, several stress-strain curves are presented, corresponding to different combinations of parameters h and η. As can be seen, in all the cases, the curve starts to deviate from a linear elastic response once the damage initiation threshold of 30 MPa was reached. At values of h and η greater than zero, material exhibits strain hardening-like response following the damage initiation. On the other hand, at values of $h < 0$ rapid stiffness reduction is observed following the initiation of damage.

Table 1
Material properties of unidirectional Seal HS160/REM/graphite/epoxy [10].

$E_{11} = 93.7$ GPa; $E_{22} = E_{33} = 7.45$ GPa
$G_{12} = G_{23} = G_{13} = 3.97$ GPa
$\nu_{12} = \nu_{23} = \nu_{13} = 0.261$
$\sigma_{2c} = 30$ MPa
$\rho = 1600$ kg/m^3

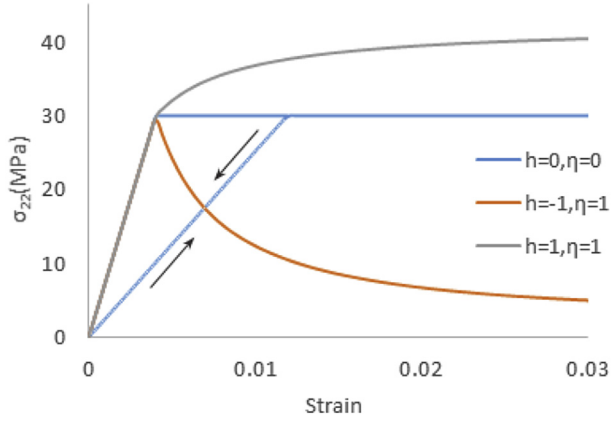

Fig. 3. Stress-strain curves obtained with a single element FE model at different values of h and η.

This is consistent with Eq. (6), which suggests that the damage threshold for further damage at every increment should reduce if h is negative, and increase otherwise. Since the values for parameters h and η were not available, to facilitate the modelling, they were assumed to be equal to zero in all the simulations, unless otherwise specified. This corresponds to ideally plastic-like material response (blue curve), also shown in Fig. 3, that gives the simplest stress-strain characterization, incorporating a degree of load carrying capacity of the cracked laminae whilst keeping the relationship as simple as possible. The unloading and re-loading scenarios are included. The effects different choices of those parameters have on the shape and the size of the damage contours will be explored in Section 3.

The value of constant k in Eq. (3), defining the reduction of shear stiffness due to damage [22], was assigned a value of $k = 0.75$. Justification for this can be found in Ref. [22] for a range of material systems where a reasonably constant value around 0.75 was identified.

2.3. The constitutive behaviour of cohesive interfaces

The elastic behaviour of the interface is defined in terms of tractions (t_n, t_s and t_t) and separations (δ_n, δ_s and δ_t) relationship, which are expressed in local coordinate system of the cohesive element as [21].

$$\begin{Bmatrix} t_n \\ t_s \\ t_t \end{Bmatrix} = \frac{1}{T}\begin{bmatrix} K_{nn} & 0 & 0 \\ 0 & K_{ss} & 0 \\ 0 & 0 & K_{tt} \end{bmatrix}\begin{Bmatrix} \delta_n \\ \delta_s \\ \delta_t \end{Bmatrix}, \tag{8}$$

where T is the thickness of the cohesive layer and K_{nn}, K_{ss} and K_{tt} represent the stiffness characteristics of the interface in normal and two perpendicular tangential directions to the interface. The interface stiffnesses are introduced as the penalty functions, which are employed to impose the relevant constraints numerically.

Damage initiation is governed by a quadratic interfacial traction criterion, which is defined as follows:

$$\left(\frac{\langle t_n \rangle}{t_n^c}\right)^2 + \left(\frac{t_s}{t_s^c}\right)^2 + \left(\frac{t_t}{t_t^c}\right)^2 = 1, \tag{9}$$

where t_n^c, t_s^c and t_t^c are the peak nominal stresses in normal and tangential directions, and $\langle\rangle$ are the Macaulay brackets.

To define the damage evolution, a power law criterion for mixed mode delamination is employed, which is given as

$$\left(\frac{G_I}{G_{Ic}}\right)^{\alpha} + \left(\frac{G_{II}}{G_{IIc}}\right)^{\beta} + \left(\frac{G_{III}}{G_{IIIc}}\right)^{\gamma} = 1, \tag{10}$$

where G_I, G_{II} and G_{III} represent the fracture energies for each of three individual modes and G_{Ic}, G_{IIc} and G_{IIIc} are their critical values. The values of exponents in Eq. (10) were chosen to be $\alpha = \beta = \gamma = 1$ [25].

The damage evolution law governs the behaviour of the interface in terms of the degradation of the interface stiffness. A non-dimensional scalar damage variable, D, is defined via linear softening scheme [21]. The material properties required for the use of cohesive elements are presented in Table 2.

After running the trial impact simulations, it became apparent that along with the delamination at the distal interface, delamination was also predicted at the proximal 0°/90° interface. This is due a shortcoming of the cohesive material model [21], which simply disregards the contribution of the compressive normal stress, allowing the shear-driven delamination to propagate unaffected by the presence of the direct compression. Various attempts have been made in the past to reduce the growth of the delamination at the proximal interface, including use of friction [14], or improved model formulation [18]. In present work, to save computational costs, the delamination at the upper interface was artificially suppressed. The effects of restraining the delamination at the upper interface on predicted delamination in the lower interface will be assessed in Section 5, where numerical results are discussed.

Unless otherwise specified, the predicted delamination patterns are presented as contours of damage variable, D, which were plotted using Abaqus post-processing tool. The threshold value $D = 0.9$ was set, so that the contour would delimit the area where nearly complete failure of the cohesive elements occurred. Comparing contours plotted over a range of the threshold values in Fig. 4(a), it can be seen that there is not much difference between the delamination areas defined by D over such a wide range of values. The transition zone from the undamaged to the fully damaged areas of the cohesive layer is relatively narrow, as can be seen in Fig. 4(b), hence the difference in delamination areas at different threshold values is insignificant.

3. Capturing the feature of pointed delamination tip

Using the finite element model as described in the previous section, low velocity impact simulations were conducted. To assess and compare the effects different methods of composite damage modelling have on the delamination predictions in the 90°/0° interface, low velocity impact simulations were conducted with three different models in the present study:

Table 2
The material properties of the cohesive layers [10].

$K_{nn} = 120$ GPa/mm; $K_{ss} = K_{tt} = 48$ GPa/mm
$t_n^c = 30$ MPa; $t_s^c = t_t^c = 80$ MPa
$G_{Ic} = 520$J/m^2, $G_{IIc} = G_{IIIc} = 970$J/m^2

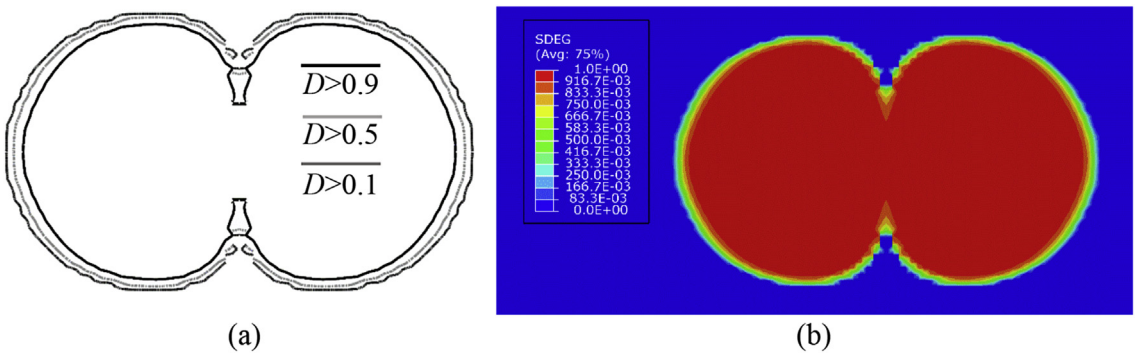

Fig. 4. Delamination pattern obtained at impact energy 2.1 J at distal 90°/0° interface: (a) contours plotted at a range of threshold values of D; (b) contour plot of the damage variable as a continuous field.

i) The response of the composite laminae was assumed to be entirely elastic and the intra-laminar damage was not accounted for in any form;
ii) Composite cracking was modelled by placing a layer of interface elements on the symmetry plane of the distal 0° lamina to allow for the discrete crack, which would have the effects of all cracks, macroscopic and microscopic, lumped to it; and
iii) CDM-based formulation, as described in Section 2.2, is employed to model the effects of intra-laminar damage.

It should be noted that approach ii) was previously employed by Aymerich et al. [10], who noted that a long crack in the distal 0° lamina was formed in the experiments and the shape of delamination was elongated 0° direction. Typical example is shown in Fig. 5(a), where delamination pattern captured experimentally [10,11] at impact energy of 6 J is presented.

The predictions obtained with three methods listed above are shown in Fig. 5(b)-(d), respectively. The delamination patterns obtained from the three models can be compared from different perspectives. A general 'peanut'-shaped pattern can be observed in all of them. However, for purely elastic composite response, delamination exhibits conspicuous rounded profile at both ends, as shown Fig. 5(b), while pointed tips at the end of each delamination lobe are apparent in Fig. 5(c), where intra-laminar damage is represented by a discrete crack. In Fig. 5(d), where the intra-laminar damage is modelled as continuum, and hence is considered dispersed, along with other minor changes, the tips changed towards pointed appearance, although not as pronounced as in Fig. 5(c).

Note that a feature of a very small surviving intact area at the centre can be observed in Fig. 5(b) at impact energy 3 J. In those elements, the values of damage variable were $D \approx 0.89$, which were just below the threshold value of $D = 0.9$. This was only observed at low impact energy.

To allow for the direct comparison of the delamination shapes obtained with different methods of modelling damage in the composite, delamination patterns calculated at impact energy 7 J are superimposed in Fig. 6. The smallest delamination area was predicted for the model which does not account for intra-lamina damage. For a model with an embedded discrete crack (yellow curve), the length of delamination is substantially larger than in the previous case, while the width remains similar. With CDM to account for intra-laminar damage, two delamination patterns are presented, which were obtained with different values of parameters h and η, defining the shape of the damage surface. In both cases, the tendency of pointed delamination tips as a distinct feature of the delamination has been captured. Along with this

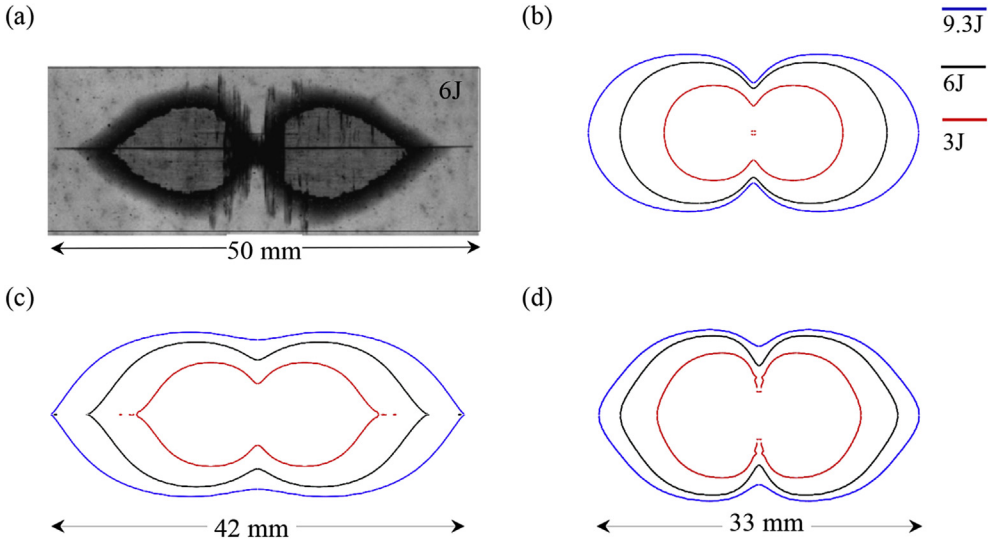

Fig. 5. Delamination pattern at distal interface: (a) X-ray image of delamination at impact energy of 6 J [11]; (b) intra-laminar damage not accounted for; (c) intra-laminar damage represented by an embedded discrete crack; (d) CDM for the intra-laminar cracking.

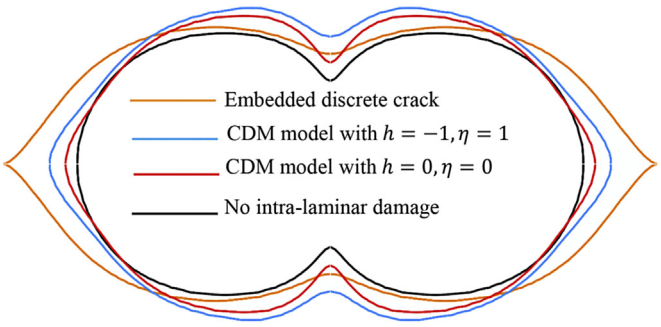

Fig. 6. Comparison of delamination patterns in the lower interface at impact energy of 7 J.

feature, the delamination area becomes larger. This increase tends to coincide with the degradation of composite stiffness as introduced by the CDM model.

Based on the analysis presented here, it can be concluded that the intra-laminar damage, i.e. the transverse matrix cracking in the 0° lamina distal to the impactor is the reason for the experimental observation of the pointed delamination tips. Without due consideration of this mode of damage, a rounded shape of delamination is predicted. Qualitatively, pointed tips of the delamination lobes can be captured by allowing intra-laminar damage development in the composite, either in form of dispersed damage, or a concentrated distinct crack. It is worth noting, however, that the latter approach has a limited predictive potential, since it implies that the location of the crack should be known in advance. As a result, its applicability to laminates of more complex lay-up cannot be assumed. Furthermore, the effects of such damage are exaggerated by a concentrated distinct crack, and a needle sharp delamination tip is predicted [10], which is not always realistic. On the other hand, it has been shown that the tendency of pointed tip subtlety can be captured simply by allowing the intra-laminar damage in the composite as a continuum. This method does not require the knowledge of the location of the transverse cracks in advance, hence can be applied to laminates of an arbitrary layup.

4. Capturing the intact zone between the lobes of delamination

Accounting for intra-laminar damage growth in the composite allows predictions of the pointed tip of the delamination area, yet it does not assist in capturing the second delamination subtlety, which is the intact zone between the lobes of delamination.

4.1. Mesh refinement

On closer inspection of this area, an anomaly was identified in the prediction of the inter-laminar shear stress τ_{13}. Along the y-axis, it should assume zero values due to the symmetry condition as prescribed in the model. However, this was not quite the case in results, as can be seen in Fig. 7(a), where a significant magnitude can be observed. It is well-known that stresses at the boundary are not generally predicted precisely from finite elements in the first place, and they are evaluated at the integration points off the boundary and extrapolated to the boundary. In presence of high stress gradient, which causes mesh sensitivity, such as the case of Fig. 7(a), significant variations in stresses are present between the boundary and the integration points closest to the boundary. It resulted in the anomaly as observed in Fig. 7(a). The issue was resolved by reducing the lengths of elements in x-direction near the centre of the plate. As can be seen in Fig. 7(b), reasonable predictions of τ_{13} were produced with a model having the mesh refined locally. Mesh refinement also improved the predictions of damage in the centre of the interface layer. Comparing the damage contours produced by the models with the uniform and the refined mesh, as shown in Fig. 8(a) at the same deformation level as that of Fig. 7, it is easy to see that delamination contour became smoother. The further mesh refinement proposed here is in order to investigate the gap between the lobes of delamination. Otherwise, the mesh as shown in Fig. 7 would be fine enough as pointed out before. In applications where this particular subtle feature of gap is not required, the proposed mesh refinement can be waived.

From the damage contour plot corresponding to the refined mesh in Fig. 8(a), the intact zone between the two lobes of delamination seems to have been captured. However, this was only the case in the early stage of delamination, or when the laminate was subjected to a low energy impact. In fact, Figs. 7 and 8(a) represent an intermediate stage of deformation at a point when the projectile energy dissipated from its incident level of 6 J to about 4.8 J. On further loading, delamination area tends to expand in all directions, as can be seen in Fig. 8(b). Towards the end of simulation, the surviving cohesive elements between the two lobes of delamination fail, the feature of intact zone disappears, and the damage contour corresponding to the model with a locally refined mesh becomes identical to that of the model with a uniform mesh. That was the reason why the necessity of further mesh refinement can be easily overlooked in the conventional mesh convergence study. Therefore, in this case, mesh refinement alone delays the propagation of delamination towards the centre of the laminate, yet does not prevent it completely.

As the direct stress transverse to the interface at centre is compressive and therefore does not contribute to delamination initiation and propagation, with transverse shear stress τ_{13} vanishing due to symmetry, the only remaining factor which may contribute to propagation of delamination at the centre of the laminate is the transverse shear stress τ_{23}. Examining the magnitude of this particular stress component, it can be found that it is not particularly high, but just high enough to trigger the delamination initiation and the subsequent propagation. A small amount of suppression will alter the outcome. This brings forward our next consideration.

4.2. Friction

Within the cohesive interface, the shear stress τ_{23} is due to relative movement of 90° and distal 0° composite laminae, and it should vanish as well at the centre owing to the symmetry. Once the cohesive elements fail and the delamination occurs, composite layers on both sides of the failed cohesive elements come into direct contact, as the central zone of the laminate is subject to compression due to the pressing load. While the compression may not be high enough to suppress the delamination from taking place, it should result in a degree of friction resisting the shear, τ_{23}.

To introduce the frictional stress, the option available in Abaqus/Explicit [21] was employed to prescribe to tangential behaviour of contact surfaces, which is based on a penalty friction formulation. This requires definition of a single friction coefficient, μ. To investigate the influence of friction on delamination propagation, a number of laminate impact cases were simulated, where friction coefficient was varied over a range as a parametric study, as presented in Fig. 9.

As can be seen, the delamination area shrinks marginally as the friction coefficient increases. The most distinctive effect of friction on shape of the delamination pattern is the necking of delamination along y-axis, which becomes narrower as the friction coefficient increases. Eventually, at the friction coefficient between 0.2

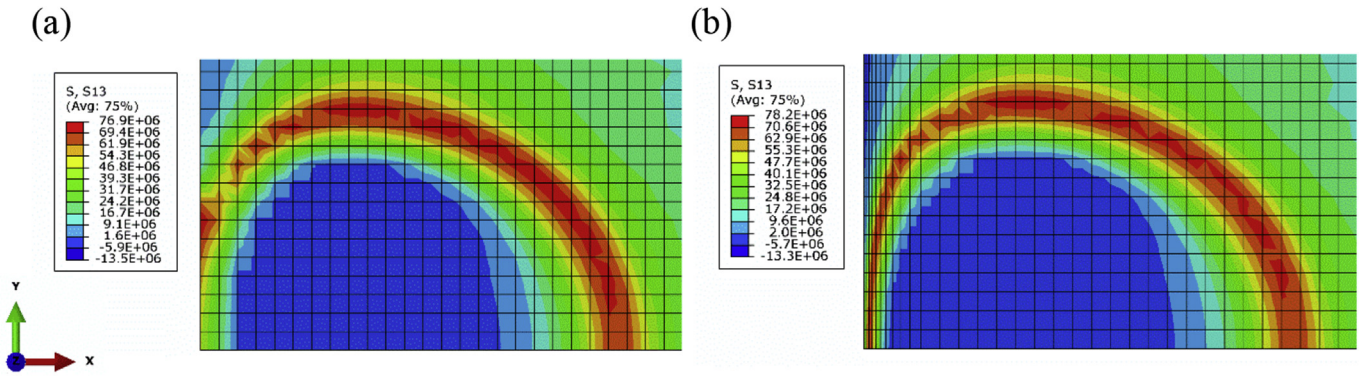

Fig. 7. Contour of shear stress τ_{13} in cohesive layer at 90°/0° interface when impact energy is 6 J: a) uniform mesh; b) refined mesh.

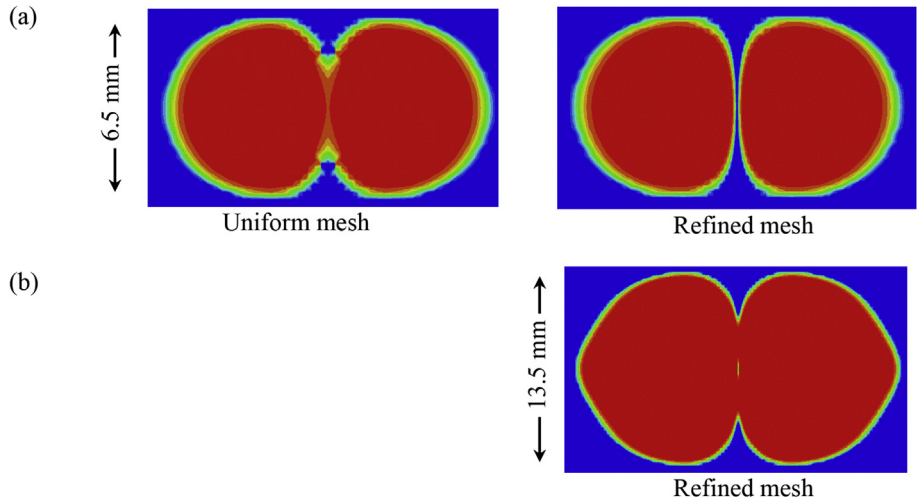

Fig. 8. Predicted delamination under 6 J impact energy: (a) comparison of the damage contours between uniform and refined meshes at the deformation level when the projectile energy has reduced to 4.8 J from 6 J (b) damage contour when projectile energy has reduced to 1.3 J from 6 J.

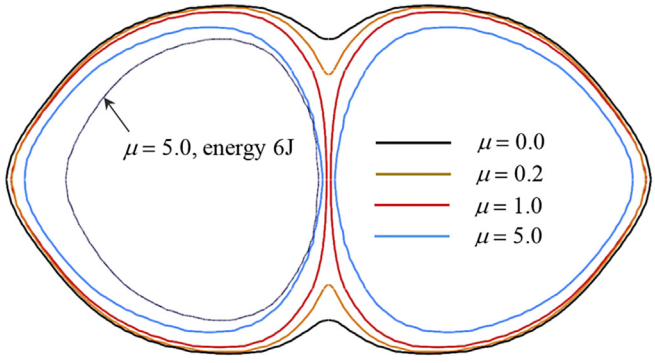

Fig. 9. Delamination patterns at different values of friction coefficients when impact energy is 9.3 J.

and 1.0, the delamination splits into two disconnected lobes. Specifically, at maximum value of friction coefficient considered here, 5.0, gap can clearly be seen between the two lobes of delamination. This indicates that the frictional stress between delaminated surfaces helps to prevent delamination from propagating into the centre. This effect can only be captured with the synergy of refined mesh and consideration of friction between delaminated plies.

For comparison, delamination lobe outline, obtained numerically, corresponding to $\mu = 5.0$ at impact energy of 6 J has also been added in Fig. 9. As expected, the size of delamination in this case is smaller than at 9.3 J, while the size of gap appears to have increased marginally.

It is worth noting that the values of friction coefficients employed here were meant to facilitate the parametric study, in absence of physically measured ones, although attempts of having them experimentally measured have been reported in the literature [26]. As there is a wide range of factors affecting the roughness of the delamination surface, such as the composite system, the interlaminar interface design and quality, the nature of the impact, the anisotropy of the friction characteristics, etc., it is not practical yet to base the analysis on measured friction coefficients. The range selected was not meant to stand physical scrutiny. Rather, it might pre-empt physical possibilities without conducting sophisticated experiments.

4.3. The width of the intact gap

Even though the gap feature can be captured by accounting for the friction in the simulation, the predicted width of the gap is relatively small as compared to that observed in the experiments [6]. The reason is believed to be the lack of localised Hertzian indentation, which cannot be reflected in models using any kind of shell elements. Such local deformation in reality allows the load to be distributed over a significantly larger area under the impactor,

and the width of the intact zone in reality is expected to be larger than that predicted. Without reverting to the formidable simulation using solid elements at a very fine mesh, an alternative is attempted by artificially increasing the diameter of the impactor, understanding that it is not a very effective way of increasing the size of the contact area.

A simulation was conducted, where the diameter of the impactor was increased to 30 mm. Delamination patterns obtained with the two sizes of the impactor are compared in Fig. 10. With the use of 30 mm impactor, the gap size increased by a factor of three, even though the absolute magnitude is still very small. The message is clear that the local distribution of the impact force over the part of the laminate underneath the impactor plays a significant role in determination of the size of the gap. With increased impactor radius, the length and the width of the delamination have also increased but only marginally.

This study indicates that the quantitative predictions of the size of the intact zone would require more accurate way of simulating the Hertzian contact between the impactor and the laminate. However, the qualitative feature of an intact zone under the impactor can be captured confidently by the synergy of incorporating the friction between the delaminated interlaminar surfaces and a reasonably refined mesh.

5. Quantitative assessment of predictions

5.1. A statement on the interpretation of experimental results

It has been demonstrated in the previous sections how the subtle features of the delamination can be captured through improved finite element modelling. Since the properties used are the material properties quoted in Ref. [10], the predictions as obtained in previous sections can be compared against the results presented there. For simplicity, the friction was not taken into account for this discussion, while the parameters involved in the intra-laminar damage model were kept the same as in Section 2.2 where the choice of these parameters has been explained.

Comparison was conducted in terms of the predicted and the measured lengths and widths of a single delamination lobe, which were plotted as functions of the impact energy in Fig. 11(a) and (b), respectively. Such comparison was also carried out by Aymerich et al. in Ref. [10], who represented composite cracking via a discrete crack in the distal 0° lamina, and reported a good agreement between the experiments and predictions. However, in Ref. [10], no specific description was given as to how the dimensions of the delamination lobes were measured. To clarify this, the authors of the present paper measured the lengths and the widths of the delamination directly from the X-ray images presented in Refs. [6,11,20]. It should be noted that the experiments described in Refs. [6,11,20] were conducted both with the stitched and non-stitched cross-ply laminate panels, and only the latter ones were used here for the measurements. As can be seen in Fig. 5(a), the delamination is defined by a thick boundary, which represents the area of partially damaged interface. For the sake of consistency, the inner clear part was considered as the delaminated area. The length and the width were measured off this particular area representing a more conservative assessment. Comparing the two sets of data in Fig. 11, it can be observed that the data corresponding to such a conservative estimate are consistently lower than the values provided in Ref. [10], which indicates that the measurements in Ref. [10] must have been taken into the thick boundary.

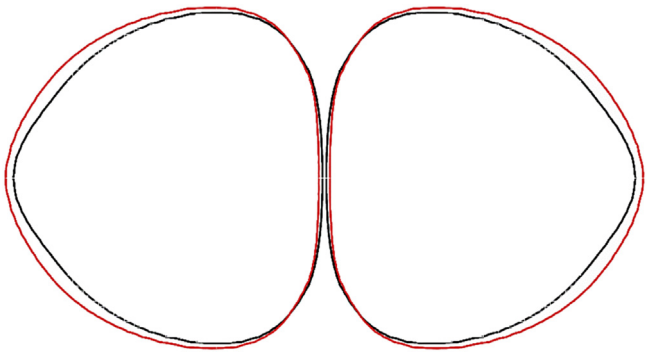

Fig. 10. Intact zone between the delamination lobes at two different diameters of the impactor (friction coefficient 1.0, impact energy 9.3 J).

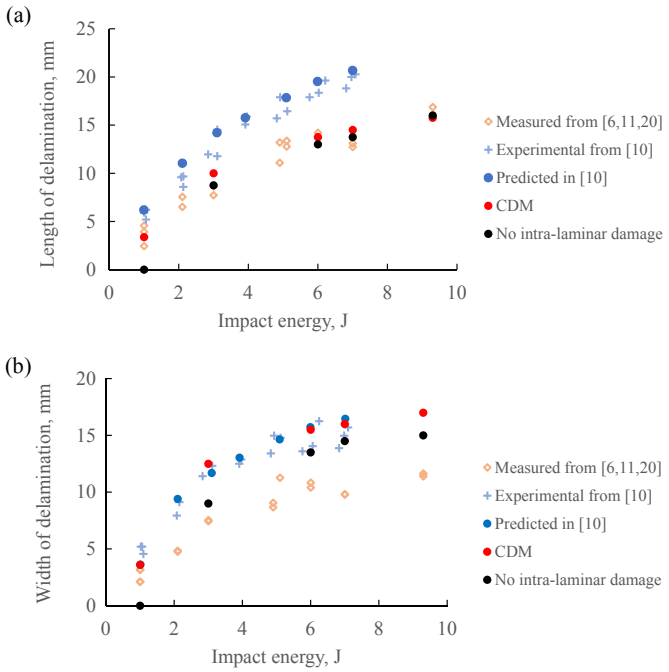

Fig. 11. Comparison of predicted and measured dimensions of delamination in 90°/0° interface: (a) length and (b) width of delamination as functions of impact energy.

The damage contours predicted with the damage threshold limit of $D = 0.9$ also represent a conservative assessment of damage, hence it is logical to compare the dimensions with the present measurements.

The effect of transverse cracking damage on delamination length was not expected to be significant, although it moderates the delamination shape with a more realistic appearance with pointed tips. As shown in Fig. 11(a), both models with and without CDM predict the length of delamination very well, with the former outperforming the latter at low values of impact energy. At the same time, both models tend to overestimate the width of delamination, as shown in Fig. 11(b). In this case, predictions obtained without CDM tended to be closer to the experimental data than those with CDM. However, since friction had not been incorporated here, which tended to compete against the effect of the intra-laminar damage on the delamination width, the inferior prediction of delamination width with the intra-laminar damage alone is understandable. In other words, the two considerations as the present paper is concentrated at, viz. intra-laminar damage and the friction on delaminated interface, have opposite effects on delamination. Therefore, taking none of them into account could result in better agreement with experiments than taking only one of them into account.

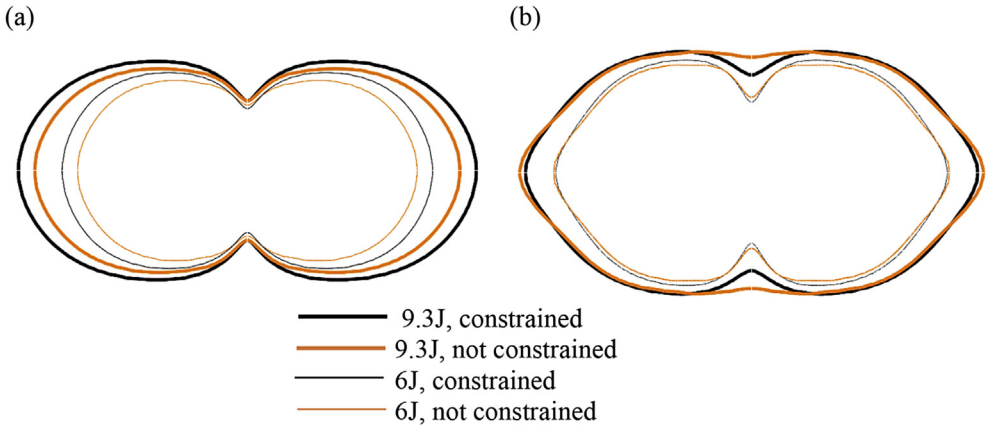

Fig. 12. Influence of constraining the proximal interface on predicted delamination in the interface: (a) model with no intra-laminar damage (a) CDM model.

The comparison as presented here demonstrates that in order to truly assess the computational accuracy of the model in terms of predicting the delamination shape and size, it is essential to establish a univocal interpretation of the measured data first. Otherwise, the comparison between the experiment and the simulation may not be meaningful.

5.2. Effects of constraining the upper interface

The influence of suppressing the delamination in the proximal interface to the impactor on predicted delamination in the distal interface is discussed briefly below. The comparison of the delamination shapes obtained with constrained and unconstrained proximal interfaces is presented in Fig. 12. As can be seen, restraining delamination in the proximal interface can indeed have an influence on the size of delamination in the distal interface. However, the effects in terms of the length and width of delamination seem to be more pronounced if the intra-laminar damage is not considered, as shown in Fig. 12(a), than if considered, as shown in Fig. 12(b). It should be noted that the emergence of delamination in the proximal interface is not always observed physically. Its appearance here was due to the lack of representation of the effects of transverse compression on the delamination initiation and propagation in the cohesive model available in Abaqus. The point to make through this exercise is to ensure the outcomes of this paper are affected neither qualitatively nor quantitatively by the suppressed proximal interface.

6. Conclusions

The reasons behind the two subtle features of delamination patterns in cross-ply laminates subjected to impact, viz. the pointed delamination fronts and an intact zone underneath the impactor, as are commonly observed experimentally, have been identified for the first time. They have been illustrated through examples with logical reasoning, such that these features can be consistently captured when the appropriate considerations for them are accounted for in the numerical model.

It has then be demonstrated clearly that the pointed delamination tips in numerical modelling are attributed to the incorporation of the intra-laminar damage, i.e. transverse matrix cracking, micro or macro, in the distal 0° lamina from the impactor. This feature can therefore be consistently captured, provided that the damage-related material properties are so given that they allow the transverse matrix cracking to take place and to evolve. Otherwise, rounded ends of delamination will be predicted.

The synergy of sufficiently refined meshes and the effects of friction between the delaminated interfaces enables the numerical model to capture the intact zone under the impactor as another subtle feature consistently observed in experiments.

The features addressed in this paper may be classified as of secondary significance as compared to the delamination area and the dimensions. However, the successful identification of the reasons behind them and the ability to reproduce them theoretically help profoundly in building up the level of confidence of theoretical prediction of delamination in a much broader sense. Based on such an enhanced level of confidence, users now can have the choice of incorporating higher levels of sophistication in order to capture features of such subtlety, when they become necessary. Alternatively, if the application concerned does not need information of this level of subtlety, one can confidently reduce the level of sophistication and hence the computational demands, yet to obtain satisfactory results suitable for the application.

Acknowledgement

The financial support for the work carried out from Beijing Institute of Aeronautical Materials (BIAM), China under Contract Number RGS 107903 is gratefully acknowledged.

References

[1] S. Abrate, Impact on Composite Structures, Cambridge University Press, UK, 1998.
[2] ASTM International Standard Test Method for Measuring the Damage Resistance of Fiber-reinforced Polymer Matrix Composite to a Drop-weight Impact Event, 2015.
[3] S. Long, X. Yao, X. Zhang, Delamination prediction in composite laminates under low-velocity impact, Compos. Struct. 132 (2015) 290–298.
[4] H.Y. Choi, F.K. Chang, A model for predicting damage in graphite/epoxy laminated composites resulting from low-velocity point impact, J. Compos. Mater 26 (14) (1992) 2134–2169.
[5] Y. Shi, T. Swait, C. Soutis, Modelling damage evolution in composite laminates subjected to low velocity impact, Compos. Struct. 94 (2012) 2902–2913.
[6] F. Aymerich, C. Pani, P. Priolo, Damage response of stitched cross-ply laminates under impact loadings, Eng. Fract. Mech. 74 (4) (2007) 500–514.
[7] R.K. Luo, E.R. Green, C.J. Morrison, Impact damage analysis of composite plates, Int. J. Impact Eng. 22 (1999) 435–447.
[8] Z. Zou, S.R. Reid, S. Li, P.D. Soden, Application of a delamination model to laminated composites structure, Compos. Struct. 56 (2002) 375–389.
[9] S. Li, S.R. Reid, Z. Zou, Modelling damage of multiple delaminations and transverse matrix cracking in laminated composites due to low velocity lateral impact, Compos. Sci. Technol. 66 (2006) 827–836.
[10] F. Aymerich, F. Dore, P. Priolo, Prediction of impact-induced delamination in cross-ply composite laminates using cohesive interface elements, Compos. Sci. Technol. 68 (12) (2008) 2383–2390.
[11] F. Aymerich, F. Dore, P. Priolo, Simulation of multiple delaminations in impacted cross-ply laminates using a finite element model based on cohesive

interface elements, Compos. Sci. Technol. 69 (11–12) (2009) 1699–1709.
[12] A. Qiu, K. Fu, W. Lin, C. Zhao, Y. Tang, Modelling low-speed drop-weight impact on composite laminates, Mater. Des. 60 (2014) 520–531.
[13] J. Zhang, X. Zhang, Simulating low-velocity impact induced delamination is composites by a quasi-static load model with surface-based cohesive contact, Compos. Struct. 125 (2015) 51–57.
[14] X. Zhang, F. Bianchi, H. Liu, Predicting low-velocity impact damage in composites by a quasi-static load model with cohesive interface elements, Aeronautical J. 116 (1186) (2012), 1367–1281.
[15] I. Guiamatsia, G.D. Nguyen, A thermodynamics-based cohesive model for interface debonding and friction, Int. J. Solids Struct. 51 (2014) 647–659.
[16] G. Perillo, N.P. Vedivik, A.T. Echtermeyer, Damage development in stitch bonded GFRP composite plates under low velocity impact: experimental and numerical results, J. Compos. Mater 49 (5) (2015) 601–615.
[17] United States Government Accountability Office, Status of FAA's Actions to Oversee the Safety of Composite Airplanes, 2011, Report to Congressional Requesters.
[18] J.P. Hou, N. Petrinic, C. Ruiz, A delamination criterion for laminated composites under low-velocity impact, Compos. Sci. Technol. 61 (14) (2001) 2069–2074.
[19] S. Abrate, J.F. Ferrero, P. Navarro, Cohesive zone models and impact damage predictions for composite structures, Meccanica 50 (2015) 2587–2620.
[20] L. Francesconi, F. Aymerich, Numerical simulation of the effect of stitching on the delamination resistance of laminated composites subjected to low-velocity impact, Compos. Struct. 159 (2017) 110–120.
[21] Abaqus Analysis User's Manual. Abaqus 6.12 HTML Documentation, 2012.
[22] S. Li, S.R. Reid, P.D. Soden, A continuum damage model for transverse matrix cracking in laminated fibre-reinforced composites, Philos. Trans. Royal Soc. A: Math. Phys. Eng. Sci. 356 (1746) (1998) 2379–2412.
[23] S. Li, R.S. Reid, P.D. Soden, M.J. Hinton, Modelling transverse cracking damage in thin, filament-wound tubes subjected to lateral indentation followed by internal pressure, Int. J. Mech. Sci. 47 (2005) 621–646.
[24] R. Talreja, A continuum mechanics characterization of damage in composite materials, Proc. R. Soc. Lond. A 339 (1985) 195–216.
[25] M. Charalambides, A.J. Kinloch, Y. Wang, J.G. Williams, On the analysis of mixed-mode failure, Int. J. Fract. 54 (1992) 269–291.
[26] J. Schön, Coefficient of friction of composite delamination surfaces, Wear 237 (2000) 77–89.